Clim. Past Discuss., 8, 4295–4332, 2012
www.clim-past-discuss.net/8/4295/2012/
doi:10.5194/cpd-8-4295-2012

Climate of the Past Discussions

The Medieval Climate Anomaly and the Little Ice Age in the Eastern Ecuadorian Andes

M.-P. Ledru[1], V. Jomelli[2], P. Samaniego[3], M. Vuille[4], S. Hidalgo[5], M. Herrera[6], and C. Ceron[6]

[1]IRD, UMR226, Institut des Sciences de l'Evolution de Montpellier (ISEM), UM2, CNRS, IRD, Place Eugène Bataillon cc 061, 34095 Montpellier cedex, France
[2]CNRS Université Paris 1, Laboratoire de Géographie, 92195 Meudon, France
[3]IRD, UMR163, Université Blaise Pascal, CNRS, IRD, Laboratoire Magmas et Volcans, 5 rue Kessler, 63038 Clermont-Ferrand, France
[4]Department of Atmospheric and Environmental Sciences, University at Albany, State University of New York, Albany, NY, USA
[5]Instituto Geofísico, Escuela Politécnica Nacional, A. P. 17-2759, Quito, Ecuador
[6]Dpto. Botanica Universidad Centrale del Ecuador (UCE), Quito, Ecuador

Received: 27 July 2012 – Accepted: 24 August 2012 – Published: 6 September 2012

Correspondence to: M.-P. Ledru (marie-pierre.ledru@ird.fr)

Published by Copernicus Publications on behalf of the European Geosciences Union.

Abstract

To better characterize the climate variability of the last millennium in the high Andes, we analysed the pollen content of a 1100-yr-old sediment core collected in a bog located at 3800 m a.s.l. in the páramo in the Eastern Cordillera in Ecuador. An upslope convective index based on the ratio between cloud transported pollen from the andean forest to the bog (T) and Poaceae pollen frequencies, related to the edaphic moisture of the páramo (P), was defined to distinguish the atmospheric moisture from the soil moisture content of the páramo. Results showed that between 900 AD and 1230 AD, the Medieval Climate Anomaly interval was warm and moist with high T/P index linked to a high ENSO variability and a weak South American Summer Monsoon (SASM) activity. Between 1230 and 1650 AD, a dry climate prevailed characterized by an abrupt decrease in the T/P index related to lower ENSO variability with significant impact on the floristic composition of the páramo. During the Little Ice Age, two phases were observed, first a wet phase between 1650 and 1750 AD linked to low ENSO variability in the Pacific and warm south equatorial Atlantic SSTs favored the return of a wet páramo, and a cold and dry phase between 1750 and 1810 AD associated with low ENSO variability and weak SASM activity resulting in drying of the páramo. The Current Warm Period marks the beginning of a climate characterized by high convective activity, the highest in the last millennium, and weaker SASM activity modifying the water stock of the páramo. Our results show that the páramo is progressively loosing its capacity for water storage and that the variability of both tropical Pacific and Atlantic SSTs matters for Andean climate patterns although many teleconnection mechanisms are still poorly understood.

CPD
8, 4295–4332, 2012

1 Introduction

The Tropics are a major climate engine for the global water cycle. In the tropical Andes, climate variability is the result of complex interactions between two main ocean-atmosphere systems over the tropical Pacific and Atlantic Oceans and submitted to strong fluctuations at interannual or decadal scales (Garreaud et al., 2009).

The understanding of the last millennium climate changes is of considerable interest as it predates the post-industrial warming or current warm period (CWP) and integrates the measured changes of the composition of the oceans and atmosphere and the nature of the biosphere of the last decades in a general context of climate variability. The recent increase in high-resolution proxy records showed that at least two main changes in global climate occurred during the last millennium. The first one or Medieval Climate Anomaly (MCA) is well recognized in both hemispheres although with some differences in timing, between 900 AD and 1250 or 1400 AD according to their location (Mann et al., 2009; Diaz et al., 2011). The second one or Little Ice Age (LIA) is characterized in function of the global glacier advance, here also with differences in timing for the age of the maximum of glacier expansion according to the location of the record, as for instance in the Andes, with a maximum around 1630–1680 AD in Bolivia and Peru and around 1730 AD in Ecuador, Colombia and Venezuela (Jomelli et al., 2009). However in the Southern Hemisphere tropics as most of the records covers a short time interval, the lack of continuous record at interannual to decadal resolution prevented from examining the long-term climate variability (e.g. Neukom and Gergis, 2011) in regions such as the Andes where populations strongly depend on mountain water resources (Bradley et al., 2006).

In Northern Ecuador, recent measurements on a glacier on the Antizana volcano established that El Niño Southern Oscillation (ENSO) is the main driver of the interannual mass balance variations of this glacier (Francou et al., 2004). However, to the north and south, in the Andes of Venezuela and the Northeastern Peruvian foothills, past records suggest that tropical Atlantic SST anomalies connected to South American

CPD
8, 4295–4332, 2012

Summer Monsoon (SASM) activity are the a major factor driving past changes in mean hydrologic conditions at these sites (Polissar et al., 2006; Reuter et al., 2009).

Past changes in ENSO variability have been recognized on lake deposition in southwestern Ecuador from spectral analysis performed on inorganic sediment laminae deposition. Results showed that ENSO were weak until 7000 cal yr BP and more frequent warm ENSO events characterized the late Holocene until 1200 cal yr BP when they progressively declined (Rodbell et al., 1999; Moy et al., 2002). During the last millennium in the equatorial Pacific lacustrine and coral records showed that these periods have been associated with La Niña-like/El-Niño-like conditions with cooler/warmer eastern equatorial Pacific and positive/negative radiative forcing respectively associated to MCA and LIA (Cobb et al., 2003; Conroy et al., 2009; Sachs et al., 2009). However these records are restricted to a particular season and make difficult comparisons with other records or long-term estimates of the climate. In addition as they are located in the equatorial Pacific Ocean the responses of the biosphere to these changes in sea surface temperature (SST) are still poorly known.

On the continent, temperature reconstructions inferred from Andean glaciers provide evidence for an MCA that was colder than today, and LIA intervals that were much colder than today which cannot easily be aligned with corresponding La Niña-like or El-Niño-like climate conditions of the tropical Pacific (Jomelli et al., 2009). Continuous continental records over the last millennium are still rare in the Andes. In Southern Peru, a pollen record attested the presence of a sustained drought between 900 AD and the early 17th century (Chepstow-Lusty et al., 2009) that allowed the Incas to expand in the whole Andean territory due to their ability to use new drought-adapted agricultural practices until high elevations (Kuentz et al., 2012). Recently, tree-ring climate reconstructions of the last 700 yr from the Central Andes also attested a persistent drought from the 14th to 16th century and return to wetter conditions from the beginning of the 17th century which was followed by another long-term drought (Morales et al., 2012). ENSO variability was inferred to explain these changes in moisture rates on the Altiplano. More to the north, in Northeastern Peru, a speleothem record showed

CPD
8, 4295–4332, 2012

a strong impact of the SASM on regional moisture of the eastern Cordillera and no drastic drought was observed for the past 2300 yr (Bird et al., 2011).

Here we present a high-resolution and continuous new pollen record that spans the last millennium. The Papallacta pollen record is located in Northern Ecuador near the city of Papallacta in the eastern Cordillera (Fig. 1). Our aim was to explore the relative importance of two dominant forcing systems and their variability in the past: the SASM because at Papallacta the seasonality is associated with the northward march of convective activity during the demise phase of the SASM, and the interannual climate variability primarily driven by ENSO in this part of the high Andes.

2 Modern settings, regional climate and vegetation

Along the Andean Cordillera, Ecuador is divided into two major hydrogeographic regions, the Pacific side, which comprises 11 % of the hydrologic supply, and the Amazon side with 89 % of the hydrologic supply. The climate in Ecuador is influenced by both Pacific and Atlantic SST (Vuille et al., 2000) with a stronger Pacific influence on the western side of the Andes and an Atlantic influence on the eastern side, thanks to the easterly jet flow which transports moist air masses from the Atlantic to the Amazon Basin (Hastenrath, 1996). However, ENSO-related changes in tropical Pacific SST also affect precipitation variability to the east of the Andes (Garreaud et al., 2009).

In normal years, the Andes between 10° N and 5° S, are characterized by a bimodal distribution of precipitation associated with the seasonal march of convective activity over the continent and latitudinal shifts of the Inter Tropical Convergence Zone (ITCZ) to the west over the Pacific. To the east precipitation seasonality is reflective of changes in seasonal moisture transport over the Amazon Basin. The southward migration of the ITCZ over the tropical Atlantic during austral summer enhances moisture influx into the SASM and induced convection over the Amazon Basin, while during the northward migration convection is weakened. Interannual variability in precipitation has been related to ENSO. Indeed SST anomalies in the tropical Pacific Ocean play an important

CPD
8, 4295–4332, 2012

role in mediating the intensity of the SASM over the tropical Andes. El Niño (La Niña) episodes are associated with below (above) average rainfall and warmer (cooler) conditions than normal in the Amazon Basin (Marengo and Nobre, 2001; Marengo, 2009). However as Western Amazon moisture rates are the highest of the whole basin (between 3000 and 3700 mm yr^{-1}) (Fig. 2), plant evapo-transpiration between the lowlands and the highlands (the glaciers at elevation above 5000 m a.s.l.) remains significant to allow an active upslope cloud convection during a below-average-rainfall year. Consequently some regions of the Eastern Cordillera are always wet because of a year-round cloud dripping.

The region delimited by Ecuador is divided into several climatic and vegetation zones as a function of the dominant air masses at different elevations. Precipitation is influenced by the seasonal displacement of the ITCZ, moving between its southernmost position near the equator and its northernmost position at 10° N causing a bimodal precipitation seasonality on the Altiplano. In the western lowlands the bimodal seasonality is strongly affected by the cold current of Humboldt and the upwelling along the coast inducing one rainy season during the austral summer (DJF). On the eastern side of Ecuador, a region that includes the Eastern Cordillera and the Amazon Basin, precipitation is controlled by the seasonal march of convective activity associated with the establishment and demise of the South American Summer Monsoon (SASM) with a dry season centered around the austral summer (JF) and winter (AS) and a rainy season during the austral automn (MAM) and spring (ON) (Fig. 2).

At Papallacta (00° 22′ S; 78° 08′ W; 3160 m), near our study area, mean annual temperature (MAT) is 9.6 °C and mean annual precipitation (MAP) is 1700 mm and often appears in the form of rain, hail, and thick fog during JJA (unpublished climate data from Instituto NAcional de Meteorologia e HIdrologia INAMHI). The seasonality is characterized by one cycle with a precipitation maximum in MJJ and a minimum in JF which is different from similar latitudes to the east (e.g. Manaus in the Amazon Basin) and the west (the Pacific coast) where the rainy season peaks during the austral summer (DJF) (CPTEC website). This is different from the Altiplano where two annual cycles

CPD
8, 4295–4332, 2012

are observed and from the Pacific coast where the rainy season is centered on the austral summer (DJF) (Fig. 2). The temperature gradient between the Amazon Basin in the lowlands (MAT 25 °C) and the high Andes (0 °C) is characterized by a steep moist adiabat along the eastern slope of the Cordillera that triggers convective activity. Consequently the MJJ peak of moisture at Papallacta is mainly a local phenomenom caused by mesoscale convective systems (Bendix, 2000; Bendix et al., 2009). In an El Niño year, when the Amazon Basin becomes warmer, upslope convective activity from plant evapo-transpiration may be enhanced producing more cloud drip at high elevations. During a positive/negative SOI a decrease/increase in precipitation is observed during the rainy season while a strong increase in precipitation is observed during a La Niña event in the dry season and no change during an El Niño event (unpublished climate data from INAMHI).

The Sucus bog at Papallacta is located near the equator (00° 21′ 30″ S; 78° 11′ 37″ W) at an elevation of 3815 m. The surrounding vegetation is composed of the bog, the páramo and the Polylepis forest. In the bog, we identified the following species: Asteraceae *Loricaria toyoides, Dorobaea pinpine/lifolia, Monticalia vaccinioides, Hippochoeris* sp., *Xenophyllum* sp., *Werneria* sp. Valerianaceae *Valeriana microphylla* Lycopodiaceae *Huperzia* sp. Gentianaceae *Gentiana sedifolia, Halemia weddeliana, Gentianella* sp. Poaceae *Cortaderia sericanta, Cortaderia nitida, Calamagrostis intermedia, Bromus* sp. Cyperaceae *Carex lechmanii* Gunneraceae *Gunnera magellanica* Ranunculaceae *Ranunculus* sp. Clusiaceae *Hypericum laricifolium, Hypericum* sp. Geraniaceae *Geranium* sp. Polygonaceae *Muehlenbeckia volcanica* Apiaceae *Hydrocotyle, Azorella* Plantaginaceae *Plantago rigida* (cushion bog). The páramo is a wet grassland located between the upper tree line and the permanent snow line. It is a constant, reliable source of high quality water for Andean regions due to the very high water retention capability of the soil. Large cities such as Quito rely almost entirely on surface water from the páramo. The páramo is located between 3600 and 4000 m with grasses dominated by plants of the Poaceae family including *Calamagrostis* and *Festuca.* Trees are mainly *Polylepis*; the most common shrubs

CPD
8, 4295–4332, 2012

are Asteraceae *Diplostephium, Pentacalia* and *Hypericaceae* (*ex Clusiaceae*) *Hypericum*. The cushion páramo located between 4000 and 4500 m mainly hosts Apiaceae *Azorella*, Plantaginaceae *Plantago Loricaria*, Asteraceae *Chuquiraga, Werneria*, and finally the desert páramo above 4500 m has Malvaceae *Nototriche*, Brassicaceae *Draba*, Asteraceae *Culcitium* and Apiaceae *Azorella*.

The forests of *Polylepis* grow in the páramo altitudinal band, i.e. between 3500 and 4300 m a.s.l., with the same climatic conditions. These forests are dominated by *Polylepis pauta* although 124 species of trees, shrubs and herbs were identified along with 25 different ferns (Romoleyroux, 2009). Among the 20 most abundant species are *Hydrocotyle bondplandii*, *Dysopsis* cf. *glechomoides Solanum ruizii*, *Miconia latifolia*, *Gunnera magellanica, Rubus coriaceus, Urtica murens*, Caryophyllaceae (*Arenaria* and *Stellaria*). Humidity is high, reaching more than 80 % in these forests.

The Upper Montane Forest grows between 3000 and ∼ 3500 m and hosts 2189 species including the following dominant ones: *Alnus, Ambrosia, Clethra, Gynoxys, Hedyosmum, Myrsine, Oreopanax, Podocarpus, Prumnopitys, Ribes, Styrax, Symplocos, Tibouchina, Weinmannia* (Jorgensen and Ulloa Ulloa, 1994).

3 Material and methods

A 9-m deep core was collected in the bog in January 2008 using a Russian corer. In this paper, we focus on the top 200 cm of the core that represents the last 1100 yr. Half sediment columns 100 cm long with a 5-cm diameter were covered by longitudinally split PVC-tubes and wrapped in plastic film. Sediment cores were sampled at 1-cm intervals and the samples were sent to different laboratories. Ash layers were identified visually, and 1–2 cm thick samples removed. After drying and sieving, the 100 or 200 µm-size fractions were selected, depending of the granulometry of each sample. Modal estimates of the main components (minerals, glass shards, lithic and pumice fragments) were obtained under a binocular microscope. The fine, glass-rich fractions were finely powdered in an agate grinder and then analyzed for major and trace elements by

CPD
8, 4295–4332, 2012

inductively coupled plasma-atomic emission spectroscopy (ICP-AES) at the *Laboratoire Domaines Océaniques, Université de Bretagne Occidentale (Brest, France)*. Relative standard deviations were ≤ 2 % for major elements, and ≤ 5 % for trace elements. We selected ICP-AES analyses over other analytical methods such as electron microprobe analysis (EMPA), because it allowed us to determine the concentrations of trace elements in the ash samples to correlate these ash layers with known volcanic eruptions in the Ecuadorian Andes.

3.1 Sediment description

The core was mostly composed of brown peat intercalated with three tephra layers (M1, M2 and M3) in the lower half of the 2-m-section, described as follows: 0–4 cm plant fungi; 4–14 cm brown-orange peat with fibers; 14–110 cm brown-black peat; 110–115 cm, M1 ash and peat layer; 115–134 cm, brown-black peat rich in vegetal fibers; 134–136 cm, mix of ash and peat; 136–144 cm, M2 ash tephra (M2a) white, biotite-rich ash; 144–150 cm tephra (M2b) coarse, gray-white, biotite-rich ash with small ash agglutinations; 150–178 brown peat with fibers; 178–181 cm tephra (M3) coarse, crystal rich ash with peat; 181–200 cm brown peat with fibers.

The M1 layer (5 cm thick) is composed of fine, yellowish ash with some mixed peat. The mineral components include plagioclase and some traces of amphibole and pyroxene, with abundant glass and pumice shards. The M2 horizon is a double layer composed of a lower (8 cm thick) and an upper (10 cm thick) horizon. The lower horizon is a gray-white coarse ash, composed of pumice fragments and ash agglutinates, as well as biotite (14 %), plagioclase, pyroxene and quartz. The upper layer is composed of fine, crystal-rich, white ash with abundant plagioclase and biotite crystals, with a small proportion of pumice fragments. Lastly, the M3 layer (3 cm thick) is coarse, crystal-rich ash, which appears to be mixed with peat. Mineral components include plagioclase (30 %), amphibole (25 %) and pyroxene (14 %), as well as pumice (27 %) and lithic (4 %) fragments.

CPD
8, 4295–4332, 2012

Bulk sample analyses of the glass-rich fractions enabled us to correlate these ash layers with known volcanic eruptions in the Northern Andes. The M2 samples are silica-rich dacites (68–70 wt. % SiO_2), whereas M3 samples correspond to siliceous andesite (60–61 wt. % SiO_2). The geochemical fields for some volcanoes have been described, namely Antisana (Bourdon et al., 2002), Cotopaxi (Hall and Mothes, 2008c), Pichincha (Robin et al., 2010; Samaniego et al., 2010) and Quilotoa volcanoes (Mothes and Hall, 2008) and may be sources of these ashes. Unfortunately, no chemical data was retrieved for sample M1.

3.2 Chronology

Dating control for core PA 1-08 is based on an empirically derived depth-age function using multiple calibration points, including six radiocarbon AMS dates and three tephra horizons. All samples for radiocarbon dating were analyzed at the French *Laboratoire de Mesure du Carbone 14* (LMC14) – UMS 2572 (CEA/DSM – CNRS – IRD – IRSN – *Ministère de la culture et de la communication*) (Table 1). Calibration of radiocarbon dates was performed by using the CALIB 6.01 and the SHcal04 Southern Hemisphere data set (Stuiver and Reimer, 1993; McCormac et al., 2004; Stuiver et al., 2011). Mean age values with the greatest probability at 1 sigma were used to create the age model with linear interpolation (Fig. 3). Geochemical analysis of the three different tephra layers of the core enabled us to identify three volcanic eruptions (Table 2): the eruption of the Guagua Pichincha between 800 and 1000 AD (Robin et al. 2008), the eruption of the Quilotoa in ~ 1270–1280 AD (Alroy et al., 2008; Mothes and Hall, 2008) and the 2nd eruption of the Guagua Pichincha in 1660 AD (Robin et al., 2008). Finally, we calibrated the radiocarbon age obtained for the Quilotoa (Hall and Mothes 2008) using the same method (CALIB 6.01, SHcal04). The resulting age model was split into three different sedimentation phases (Fig. 3). The base of the core was calculated to be 947 AD.

CPD
8, 4295–4332, 2012

3.3 Pollen analysis

Pollen samples were prepared using a standard protocol (Faegri and Iversen, 1989) and mounted in silicone oil on microscope slides. Pollen analyses were performed under 600X magnification. Pollen grains and spores were identified using our reference pollen collection and pollen keys (Hooghiemstra, 1984; Ortuño, 2008; Kuentz, 2009; Herrera, 2010). A minimum of 300 terrestrial pollen grains was analyzed in each sample. Fern spores and aquatic or water level-related taxa were excluded from the total sum for percentage calculation. Spore frequencies were calculated as a proportion of the total pollen sum. The pollen record was plotted using Psimpol (Bennett, 1994) and divided into zones on the basis of constrained cluster analysis by sum of squares analysis (CONISS) with pollen taxa ≥ 1 % (Grimm, 1987) (Fig. 5). The pollen concentration was calculated using the method of Cour (1974). Sample resolution is ∼ 14 yr.

Surface samples consisting of several pinches of the surface layer of soil were collected at 100 m intervals along a transect between the surface of the glacier at 4500 m a.s.l. where two samples were analyzed, and the coring site at 3800 m, plus two samples in the *Polylepis* forest located at the edge of the bog and in the páramo surrounding the bog (Fig. 4a).

3.4 Transported pollen/Poaceae (T/P) ratio as convectivity index

Changes in relative abundance between the cloud transported pollen taxa from the Andean forest, *Alnus, Hedyosmum, Podocarpus*, and the Poaceae, as a function of edaphic moisture at this high elevation, can be effectively captured by the ratio of pollen percentages between the Transported taxa and the Poaceae, i.e. the T/P ratio (e.g. Liu et al., 2005). Based on modern ecology and the geographical distribution of these taxa, the T/P ratio can be used as a proxy for upslope cloud convectivity below the bog. Indeed, grasses of the páramo are shallow-rooted plants that proliferate in wetter conditions (Liu et al., 2005). The two different expressions of moisture are reflected in the distinct altitudinal transect of the modern pollen rain (Fig. 4a, b). Consequently, we

CPD
8, 4295–4332, 2012

can use the logarithmic T/P ratio as a convectivity index for the Eastern Cordillera. Accordingly, the T/P ratio would be 0 if the transported and Poaceae percentages are equal. Positive numbers indicate the dominance of cloud transported pollen and therefore higher convective transport of the Andean forest pollen grains and significant cloud drippping as a source of moisture. Negative values (abundance of Poaceae) suggest the presence of permanent humidity in the soil of the páramos.

4 Results

4.1 Modern pollen rain

Results are presented in Fig. 4a, b and commented from low to high elevations.

The upper montane forest taxa are represented by *Alnus, Hedyosmum* and *Podocarpus*. These taxa do not grow in the area around the bog today but 200 m below, at 3600 m a.s.l. What is extremely surprising is that their highest frequencies were observed at a high elevation, near the glacier. This observation attests to strong pollen transport today from the Andean forest limit at ~ 3600 m a.s.l., until the glacier located at 4500 m a.s.l. as observed in Bolivia (Ortuño et al., 2011). This observation confirms the fact that convective activity can be characterized by the frequency of these three taxa and the use of the index of convective T/P activity defined above.

Ambrosia arborescens is the only species of *Ambrosia* that grows on the Eastern Cordillera at the latitude of Papallacta. It is an herb growing between 3000 and 3400 m a.s.l. in Northern Ecuador, in the upper montane forest ecosystem, where MAP ranges between 600 to 1700 mm yr^{-1} and MAT between 9 °C and 12 °C (Jorgensen and Leon-Yanez, 1999). The plant is insect pollinated, meaning that the pollen grains are not dispersed over long distances.

Polylepis pollen grains are well represented in the *Polylepis* forest close to the bog, and are not transported. For that reason, they are considered as good indicators of the proximity of a forest.

CPD
8, 4295–4332, 2012

In the bog, modern pollen deposition is defined from the top of the fossil record (Fig. 6) and is characterized mainly by Poaceae, Ericaceae, *Geraniella* and *Huperzia*.

Poaceae and Asteraceae type *Senecio* pollen grains characterize the páramo. Poaceae is mainly represented by *Calamagrostis,* an herb able to retain water in the soil and which gives the Páramo its water storage capacity. When Asteraceae type *Senecio* becomes dominant, it is interpreted as drier conditions on the páramos (Reese and Liu, 2005).

Apiaceae pollen frequencies increase at high elevation. Two genera of the Apiaceae family are able to grow above 4000 m, *Oreomyrrhis andicola*, an herb that grows at 4500 m and, *Ottoa oenanthoides* an herb that grows between 4000 and 4500 m (Jorgensen and Ulloa Ulloa, 1994; Jorgensen and Leon-Yanez, 1999). They are both indicators of cold temperature, as the base of the glacier is located at 4500 m a.s.l. today. Melastomataceae is an ubiquist shrub or herb.

Hence, changes in Poaceae frequencies are associated with year-round moisture on the páramo and the ability of the grassland to store water while the convectivity index provides information about changes in the intensity of upslope cloud activity or convective activity related to the temperature gradient between the Amazon Basin and the above glaciers.

4.2 Fossil record

The results of PA 1-08 pollen record are detailed in Table 3 and presented in a synthetic figure along a depth scale (Fig. 5) showing the key taxa identified in the surface samples (Fig. 4). Four main taxa or groups of taxa are distinguished to characterize either moisture or temperature changes on the páramo: Poaceae, Apiaceae, *Ambrosia* and Arboreal Pollen taxa (AP). They are represented along a time scale (Fig. 6). Total pollen concentration fluctuated between 100 and 2000 grains g^{-1} with the lowest value between ~ 1230 and 1650 AD.

CPD
8, 4295–4332, 2012

5 Environmental reconstructions

Today, the upper montane forest grows up to ~ 3500 m and the pollen record of Guandera showed that the forest has never reached the altitude of the bog in the past 3000 yr (Moscol Oliveira and Hooghiemstra, 2010). Therefore we can assume that in the last 1000 yr all the tree taxa indicators of forest, *Alnus, Hedyosmum*, *Podocarpus*, were always transported from their source by cloud convection and deposited on the bog by cloud drip and rainfall.

5.1 The period 900 to 1230 AD

This period includes two volcanic eruptions, one in 1035 AD and one in 1220 AD.

The high frequencies of *Ambrosia* attest to locally humid climatic conditions and warm temperatures. A drier interval occurred between ~ 1050 and 1150 AD when *Ambrosia* decreased drastically. Tree taxa are mainly represented by Melastomataceae which also grow as shrubs in the area around the bog. The upper montane forest taxa are well represented in both frequency and concentration providing evidence of convective activity (Fig. 6). Two colder episodes (increase in Apiaceae) occurred in ~ 1080 AD and ~ 1230 AD. Poaceae frequencies are high and attest to permanent wet soil on the páramo and to the presence of a wet mean state climate.

5.2 The period 1230 to 1650 AD

The very low frequencies of transported taxa and *Ambrosia*, the dominance of Melastomataceae and Poaceae, and the low convectivity index characterize different climatic conditions from the previous interval with no upslope convectivity and different local moisture. This is confirmed by a different landscape suggested by the expansion of the *Senecio* type of Asteraceae. This landscape could also correspond to a post eruptive situation. However, the long duration of this event (~ 460 yr), the absence of tephra and the slow sedimentation (0.03 cm yr^{-1}) (Fig. 4) during this interval support the hypothesis

CPD
8, 4295–4332, 2012

that this anomaly is climatically driven. Poaceae is found at lower frequencies than during the previous interval also attesting to less moisture. This is the driest interval of the record due to a much reduced upslope convective activity.

5.3 The period 1650 to ~ 1750 AD

This interval includes one volcanic eruption in 1660 AD.

The return to upslope convective activity and wetter climate is evidenced by the simultaneous increase in tree frequencies, convectivity index and Poaceae. The presence of the species association, Poaceae, Ericaceae, *Geraniella*, Urticales, *Huperzia*, reflects the spectrum of the bog surrounded by the grass páramo. A colder episode occurred during this interval as evidenced by the increase in Apiaceae between 1640 and 1670 AD. Both high Poaceae frequencies and convective index attest to high moisture rates on the páramo.

5.4 The period ~ 1750 to 1810 AD

Until 1780 AD, the decrease in Poaceae was balanced by the progressive expansion of Apiaceae and *Ambrosia* revealing the begining of a cooler climate on the páramo. The presence of *Ambrosia* at 3815 m a.s.l. shows that moisture rates were higher than today, while the presence of Apiaceae attests to cooler temperatures. The convectivity index increased progressively throughout the zone. Between 1780 and 1810 AD, the simultaneous regression of *Ambrosia* and Poaceae, and the maximum expansion of Apiaceae attest to a drier páramo due to a drier and colder climate than before, in fact, the coldest and the driest of the entire PA 1-08 record.

5.5 The period 1810 to 1850 AD

The progressive regression of Apiaceae attests to the return of warmer temperatures. The marked increase in tree pollen frequencies was due to a significant increase in upslope convective activity as the position of the upper tree line did not change during

CPD
8, 4295–4332, 2012

this period (Moscol Oliveira and Hooghiemstra, 2010), which was confirmed by the convectivity index (Fig. 7). The return of *Ambrosia* characterized the humid soil around the bog, which was also evidenced by the presence of bog-associated taxa. Poaceae frequencies remained low. This confirmed that changes in soil capacity for water stored observed in the previous interval are continuing. This interval was warmer with stronger convective activity than before.

5.6 The period 1850 to 2008 AD

Ambrosia frequencies remained stable; Apiaceae continued to decrease and became rare in the spectrum, a significant expansion of *Huperzia* and an increase in the frequencies of upper montane forest trees and in the convectivity index attesting to warmer temperatures in the area and to the significant contribution of the upslope convective activity to moisture rates in the high Eastern Cordillera. Here again, the lower frequencies of Poaceae attest to less water in the soil of the páramos than in the previous interval.

The period between 1810 and 2008 AD characterized the strongest upslope convective activity of the whole record and the lowest water stock in the soil of the páramos in the past 1000 yr.

5.7 The impact of volcanic eruptions on the vegetation

None of the three volcanic eruptions recorded in the bog originated from Antizana volcano. The long distance from Quilotoa to the study area (more than 100 km from the bog) probably protected it from significant changes in the vegetation and landscape although pre-Colombian sites in Northern Ecuador were abandoned after the eruption (Hall and Mothes, 2008). Indeed, the 18-cm thick ash layer from the Quilotoa completely dried up the bog for a decade and slowed down the pollination rates, evidence that the plants were suffering. *Gunnera* showed high frequencies (11 %) after the deposition of the tephra M2. This herb is associated with stagnant water and could be

CPD
8, 4295–4332, 2012

a sign of a change in the drainage of the bog for a decade after the eruption, when the regional climate remained moist. A peak in Urticales (11 %) was observed after the M1 eruption.

5.8 The response of the *Polylepis* forest

Today the *Polylepis* forest is well represented in the páramo all around the bog. The fossil pollen record shows that the forest was always present and reacted very little to the climate changes that occurred during the last 1000 yr. *Polylepis* frequencies decreased from 4 % to 0.2 % in the years following the eruption but returned to their initial values quite rapidly.

Six distinct changes in the behavior of the páramo and its associated climate occurred at Papallacta during the last 1000 yr. The first one happened between 900 and 1230 AD, and was characterized by the alternance of moist and dry episodes and a warmer climate than today, with upslope convective activity and a seasonal climate during which the páramo was wet. During the second one, between 1230 and 1650 AD, convective activity stopped abruptly at the same time as there was an expansion of Asteraceae characterizing a drier páramo. The third climatic phase, between 1650 AD and 1750 AD, was characterized by a sharp increase in Poaceae and the return of the convective moisture attesting a wet period; the páramo was drier and probably less extensive than previously. The coldest episode of the record occurred between 1750 and 1810 AD when the páramo became drier. During the fifth climate change, after 1810 AD, upslope convective activity increased significantly with two steps, before and after 1810 AD, and temperatures became progressively warmer, while the páramo remained drier, attesting to less water stored in the soil in spite of the high convective activity.

CPD
8, 4295–4332, 2012

6 Discussion

Among these six climate intervals, the MCA, the LIA and the CWP are clearly visible in the Papallacta pollen record. They are characterized by significant variability of rainfall and temperature with pronounced century-scale changes in the mean state climate during the MCA, one intermediate period between the MCA and the LIA, the two-step LIA and the CWP.

To detect the major determining factor of precipitation and temperature at Papallacta, either related to the Pacific or Atlantic SSTs, we plotted the convective index with changes in the ratio of tychoplanktonic to epiphytic diatoms, the T/E index, associated to changes in number of El Niño events from the El Junco lacustrine record in the Galapagos (Conroy et al., 2009) and changes in precipitation strictly linked to SASM activity from the Cascayunga speleothem record in Northeastern Peru (Bird et al., 2011). These comparisons reveal a remarkable link between the Papallacta convective index and the Eastern Equatorial Pacific SST T/E index (Fig. 7). High values of T/E index were related to a high number of El Niño events. However modern climate analysis showed that during the negative phase of the ENSO, when temperatures are cooler in the equatorial Pacific, a drier climate is observed on the Altiplano (Vuille et al., 2000; Garreaud et al., 2009). Therefore, as available reconstructions of the past millennium showed different patterns of changes, the link between high number of El Niño events and moist long-term climate on the Altiplano is questionnable. In addition, at El Junco, the diatom-based Eastern Equatorial Pacific SST T/E index does not relate neither the La Niña-like MCA nor the El-Niño-like LIA defined from coral reconstructions (Cobb et al., 2003; Sachs et al., 2009) but rather the frequency of the events and the variability of the considered time period. This interpretation is supported by recent results obtained from spectral analysis based on tree-ring records in the Central Andes (Morales et al., 2012). Indeed they showed that ENSO variability was more important for long-term climate expression than considering separatedly the number of El Niño–La Niña events. Consequently we interpreted the remarkable link between T/P index

CPD
8, 4295–4332, 2012

at Papallacta and T/E index at El Junco as reflecting the variability of Pacific SSTs rather than the number of El Niño events.

6.1 The Medieval Climate Anomaly

Early in the millennium, the tropical Pacific was shown to be cooler, which is consistent with La Niña-like conditions (Cobb et al., 2003). Consequently, under the assumption of a La Niña-like climate in the equatorial Pacific during the MCA, referring to modern observations would lead us to expect an expansion of Antizana glacier between 900 and 1200 AD (Francou et al., 2004). However, a downslope shift in the glacier front was not confirmed by the pollen record. On the other hand, the same modern climate observations also show that the negative SOI or La Niña events are able to increase winter (JJA) and summer (DJF) moisture on the páramo. Consequently it appears that at Papallacta, the high convective index in phase with the increased ENSO frequency reveals an increase in moisture induced by a decadal-scale modulation of ENSO-related climate variability. In addition, high Poaceae frequencies attest to permanently wet soil on the páramo. The MCA is characterized by a warm Northern Equatorial Atlantic (Haug et al., 2001) and a cool South Equatorial Atlantic (Polissar et al., 2006) (Fig. 1). This feature led to a decrease in rainfall in the Amazon Basin during the Amazonian wet season (DJF) (Cohen et al., 2009) associated with a northern migration of the ITCZ and a weakened SASM (Cohen et al., 2009; Reuter et al., 2009). Our results show that at the elevation of Papallacta the lack of moisture induced by a weakened SASM was probably counterbalanced by the high ENSO variability.

Model reconstructions show a division between the Northern and Southern Tropical Andes during the MCA, with wetter/drier climate to the north/south (positive/negative soil anomaly) in agreement with our results (Seager et al., 2008; Diaz et al., 2011). Consequently under negative soil moisture conditions, the southern páramo would have been drastically reduced in size. This is an important boundary to take into consideration when predicting the impact of climate warming on the water supply from the páramo.

CPD
8, 4295–4332, 2012

6.2 The period 1250 to 1650 AD

Although this period is well characterized at Papallacta, all the other records divided the beginning of this period (up to 1400 AD) as part of the MCA and the second part (between 1500 and 1650 AD) as the beginning of the LIA. Our subdivision at Papallacta is based on evidence for the absence of cloud convection that is likely specific to the Eastern Cordillera. Comparison between the convective index and ENSO frequencies shows a decrease in both phenomena (Fig. 7). The combined effect of a weaker SASM (Reuter et al., 2009) and low ENSO frequencies at the beginning of the interval (Conroy et al., 2009) created particularly dry conditions at Papallacta that modified the landscape. After 1300 AD, ENSO frequencies were still low when the SASM became stronger (Bird et al., 2011). The presence of both Poaceae and Asteraceae taxa attest to the fact that the páramo was drier but still functioning as a wet grassland. More to the south, in the Central Andes, frequent extreme droughts were observed until 1400 AD and less frequent extreme droughts until 1600 AD (Morales et al., 2012) and were related to low variance ENSO variability. Also in the Southern Andes, the period between 1250 and 1400 AD, was defined as the driest phase of the MCA with a weak correlation with ENSO (Boucher et al., 2011; Neukom and Gergis, 2012). Our results confirm that this extreme drought was a general long-term climate pattern from equator to Southern Andes.

6.3 The Little Ice Age

In the equatorial Pacific, the time interval corresponding to the LIA ~ 1500 to 1800 AD is characterized by the warming of the SST associated with El Niño-like conditions (Sachs et al., 2009). Today, at high elevations, an El Niño event is associated with warmer temperatures and negative glacier mass balance (Francou et al., 2004). However, glacier retreat due to mean state El-Niño-like condition, would cause an upslope shift of the vegetation altitudinal band, which is not the case at Papallacta. On the contrary, the growth of Apiaceae reached the lower altitude of 3800 m a.s.l. indicating to

CPD
8, 4295–4332, 2012

a downslope shift of the glacier and a decrease in temperature. Given the high convective index and low ENSO variability between 1650 and 1750 AD, (Fig. 7) we conclude that the wetter climate conditions observed at Papallacta responded to both low ENSO variability and stronger SASM activity rather than an El Niño-like mean state assumption.

In the Atlantic, a cool Northern Equatorial Atlantic (Haug et al., 2001) as opposed to a warm Southern Equatorial Atlantic (Polissar et al., 2006) caused a southward shift of the ITCZ. This century-scale ocean-atmosphere coupling was characterized by the intensification of the SASM and increased precipitation in tropical South America (Vimeux et al., 2009; Bird et al., 2011) and particularly a wetter Amazon Basin (Cohen et al., 2009; Vuille et al., 2012) and the presence of moisture along the Eastern Cordillera in Northern South America until at least Southern Peru (Reuter et al., 2009; Bird et al., 2011). The combined effect of a stronger SASM and low ENSO variability favored the highest moisture rates of the last 1000 yr, with a maximum of ice expansion in $\sim$1730 AD characterized by a $\sim 2\,^{\circ}$C drop in temperature and a 20 % increase in precipitation (Jomelli et al., 2009).

At Papallacta, this pattern ended between 1750 and 1810 AD. Indeed the sharp decrease in Poaceae frequencies (Fig. 6) indicates drier conditions on the páramo linked to a decrease in the permanent moisture rates of the soil. This interval included the driest and coldest phase at Papallacta. A weakened SASM system probably related to the beginning of the northward shift of the ITCZ (Haug et al., 2001), a high upslope convection as the Amazon Basin was very wet, associated to low ENSO frequencies characterized the climate system of the second part of the LIA.

6.4 The Current Warm Period

After 1810 AD, the abrupt increase in the convective index, which reached its highest values in the last 1000 yr, reflects the sharp increase in the intensity of cloud dripping up to high elevations. Here again the vegetation belt characterized by the progressive

CPD
8, 4295–4332, 2012

retreat of Apiaceae and the return of warmer temperatures in the bog were in phase with the retreat of the glacier Antizana.

The warming of the Pacific and the increase in ENSO variability (Conroy et al., 2009; Morales et al., 2012) led to significant glacier retreat 1800 AD (Francou et al., 2000; Jomelli, et al., 2009). The continuous decrease in Poaceae attests to drier soil and changes in precipitation regimes under the combined effect of weaker SASM and higher ENSO variability. The páramo drastically weakened progressively losing its ability to store water and to provide a supply for the socio-economic activities in the surrounding area although atmopsheric moisture was high.

At the glacier above, a two-step warming, with a slow phase that lasted until 1880 AD, and a rapid phase from 1880 to 2008 AD was observed (Jomelli et al., 2009). A high convective index reaching the highest elevation, also recorded in our modern pollen samples (Fig. 4b), is probably evidence for a precipitation increase during the last two centuries. This precipitation increase, however, was insufficient to induce a glacial advance. On the contrary, glaciers started to retreat after 1810 AD, in conjunction with the industrial warming and under the combined effect of an increase in ENSO variability, higher local convective activity, and a weaker overall SASM.

7 Conclusions

The Papallacta pollen record highlights the influence of Pacific SSTs variability and Atlantic SST gradient anomalies on moisture rates and temperature for the last 1000 yr in the high Ecuadorian Andes. Indeed, the interplay of the Pacific and Atlantic SST anomalies, respectively associated with ENSO variability and SASM activity, provided two modes of variability in the mean state climate that influenced the rainfall distribution at high elevations. It appears the variability of equatorial Pacific SST anomalies is closely linked to convective activity along the eastern slopes of the Cordillera although teleconnection mechanisms are still poorly understood. The MCA was characterized by strong Pacific SST variability and weaker SASM until 1230 AD; between the MCA

CPD
8, 4295–4332, 2012

and the LIA, 1230 to 1650 AD, low ENSO frequencies and cool south equatorial Atlantic SSTs led to a drier páramo. During the LIA, two phases were observed, the first one between 1650 and 1750 AD linked to low ENSO variability in the Pacific and warm south equatorial Atlantic SSTs favoring the return of a wet páramo, the second one between 1750 and 1810 AD associated with low ENSO variability and weak SASM activity resulting in drying of the soil of the páramo. The CWP marked the beginning of a climate characterized by high ENSO frequencies, the highest in the last millennium, and weak SASM activity which accelerated the glacier retreat (Favier et al., 2004) and weakened the páramo. In addition, our results show that the páramo started to weaken in 1750 AD during the coldest phase of the LIA and did not recover during the CWP, hence loosing its high water storage stock potential. Our results also show that the variability of both tropical Pacific and Atlantic SSTs matters for Northern Andean climate patterns.

In the 21st century, areas of increased and decreased precipitation are projected for the tropical Andes, although these are spatially incoherent (Urrutia and Vuille, 2009). On the eastern slopes of the Andes, the observed upwards convective activity (this study), the projected warming at higher altitudes (Bradley et al., 2006) and the predicted increase in precipitation up to 2000 m a.s.l. (Urrutia and Vuille, 2009) will challenge social-economic activities, including the supply of drinking water, and of water for agriculture and for the production of hydropower. Indeed, the accelerated melting of the glacier is not the only threat to water stocks in the 21st century: the change in the hydrology of the páramo that started at the end of the 18th century will have much more drastic long-term impacts on water supplies to communities living the tropical Andes and in all hydrologically related lowlands (Buytaert et al., 2006).

Acknowledgement. This research is part of the UR GREAT ICE program at IRD, ANR ESCARCEL and ANR EL PASO. Financial support was provided by IRD and the French ANR. All radiocarbon dates were measured at the *Laboratoire de Mesure du Carbone 14* (LMC14) – UMS 2572 (CEA/DSM CNRS IRD IRSN). We thank the *Ministerio del Ambiente del Ecuador* for permitting and facilitating our fieldwork at Papallacta, the INAMHI for providing climate data, and we are grateful to Boromir and Jörg Bogumil for their help during fieldwork.

CPD
8, 4295–4332, 2012

References

Alroy, J., Aberhan, M., Bottjer, D. J., Foote, M., Fürsich, F. T., Harries, P. J., Hendy, A. J. W., Holland, S. M., Ivany, L. C., Kiessling, W., Kosnik, M. A., Marshall, C. R., Mcgowan, A. J., Miller, A. I., Olszewski, T. D., Patzkowski, M. E., Peters, S. E., Villier, L., Wagner, P. J., Bonuso, N., Borkow, P. S., Brenneis, B., Clapham, M. E., Fall, L. M., Ferguson, C. A., Hanson, V. L., Krug, A. Z., Layou, K. M., Leckey, E. H., Nürnberg, S., Powers, C. M., Sessa, J. A., Simpson, C., Tomasoviych, A., and Visaggi, C. C.: Phanerozoic trends in the global diversity of marine invertebrates, Science, 321, 97–100, 2008.

Bendix, J.: Precipitation dynamics in Ecuador and Northern Peru during the 1991/92 El Niño: a remote sensing perspective, Int. J. Remote S., 21, 533–548, 2000.

Bendix, J., Trachte, K., Cermak, J., Rollenbeck, R., and Nauss, T.: Formation of convective clouds at the foothills of the Tropical Eastern Andes (South Ecuador), J. Appl. Meteorol. Clim., 48, 1682–1695, 2009.

Bird, B. W., Abbott, M. B., Vuille, M., Rodbell, D. T., Stansell, N. D., and Rosenmeier, M. F.: A 2,300-year-long annually resolved record of the South American summer monsoon from the Peruvian Andes, P. Natl. Acad. Sci., 108, 8583–8588, 2011.

Boucher, É., Guiot, J., and Chapron, E.: A millennial multi-proxy reconstruction of summer PDSI for Southern South America, Clim. Past, 7, 957–974, doi:10.5194/cp-7-957-2011, 2011.

Bourdon, E., Eissen, J. P., Monzier, M., Robin, C., Martin, H., Cotten, J., and Hall, M. L.: Adakite-like lavas from Antisana Volcano (Ecuador): evidence for slab melt metasomatism beneath the Andean Northern Volcanic Zone, J. Petrol., 43, 199–217, 2002.

Bradley, R. S., Vuille, M., Diaz, H. F., and Vergara, W.: Threats to water supplies in the Tropical Andes, Science, 312, 1755–1756, 2006.

Buytaert, W., Célleri, R., De Bievre, B., Cisneros, F., Wyseure, G., Decckers, J., and Hostede, R.: Human impact on the hydrology of the Andean paramos, Earth Sci. Rev., 79, 53–72, 2006.

Chepstow-Lusty, A. J., Frogley, M. R., Bauer, B. S., Leng, M. J., Boessenkool, K. P., Carcaillet, C., Ali, A. A., and Gioda, A.: Putting the rise of the Inca Empire within a climatic and land management context, Clim. Past, 5, 375–388, doi:10.5194/cp-5-375-2009, 2009.

Cobb, K. M., Charles, C. D., Cheng, H., and Edwards, L.: El Niño/Southern Oscillation and tropical Pacific climate during the last millennium, Nature, 424, 271–276, 2003.

CPD
8, 4295–4332, 2012

Cohen, M. C. L., Behling, H., Lara, R. J., Smith, C. B., Matos, H. R. S., and Vedel, V.: Impact of sea-level and climatic changes on the Amazon coastal wetlands during the late Holocene, Veg. Hist. Archaeobot., 18, 425–439, 2009.
Conroy, J. L., Restrepo, A., Overpeck, J. T., Steinitz-Kannan, M., Cole, J. E., Bush, M. B., and Colinvaux, P. A.: Unprecedented recent warming of surface temperatures in the Eastern Tropical Pacific Ocean, Nat. Geosci., 2, 46–50, 2009.
Cour, P.: Nouvelle techniques de détection des flux et des retombées polliniques: étude de la sedimentation des pollens et des spores à la surface du sol, Pollen et Spores, XVI, 103–141, 1974.
Diaz, H. F., Trigo, R., Hughes, M. K., Mann, M. E., Xoplaki, E., and Barriopedro, D.: Spatial and temporal characteristics of climate in medieval times revisited, B. Am. Meteorol. Soc., 92, 1487–1500, 2011.
Faegri, K. and Iversen, J.: Textbook of Pollen Analysis, 4th Edn., J. Wiley & Sons, Chichester, UK, 1989.
Favier, V., Wagnon, P., and Ribstein, P.: Glaciers of the outer and inner tropics: a different behaviour but a common response to climatic forcing, Geophys. Res. Lett., 31, L16403, doi:10.1029/2004GL020654, 2004.
Francou, B., Ramírez, E., Cáceres, B., and Mendoza, J.: Glacier evolution in the tropical Andes during the last decades of the 20th century: Chacaltaya, Bolivia, and Antizana, Ecuador, Ambio, 29, 416–422, 2000.
Francou, B., Vuille, M., Favier, V., and Cáceres, B.: New evidence for an ENSO impact on low-latitude glaciers: Antizana 15, Andes of Ecuador, 0°28′ S, J. Geophys. Res., 109, D18106, doi:10.1029/2003JD004484, 2004.
Garreaud, R. D., Vuille, M., Compagnucci, R., and Marengo, J.: Present-day South American climate, Palaeogeogr. Palaeocl., 281, 180–195, doi:10.1016/j.palaeo.2007.10.032, 2009.
Hall, M. A. and Mothes, P. A.: Volcanic impediments in the progressive development of pre-columbian civilizations in the Ecuadorian Andes, J. Volcanol. Geoth. Res., 176, 344–355, 2008.
Hastenrath, S.: Climate Dynamics of the Tropics, Kluwer Academy, Dordrecht, 1996.
Haug, G. H., Hughen, K. A., Sigman, D. M., Peterson, L. C., and Röhl, U.: Southward migration of the intertropical convergence zone through the Holocene, Science, 293, 1304–1306, 2001.

CPD
8, 4295–4332, 2012

Herrera, M.: Polen y esporas del Bosque de Papallacta, Biologia, Universidad Centrale del Ecuador (UCE), Quito, 120 pp., 2010.
Hooghiemstra, H.: Vegetational and Climatic History of the High Plain of Bogotá, Colombia: a Continuous Record of the Last 3.5 Million Years, J. Cramer, Vaduz, 1984.
Jomelli, V., Favier, V., Rabatel, A., Brunstein, D., Hoffmann, G., and Francou, B.: Fluctuations of glaciers in the tropical Andes over the last millennium and paleoclimatic implications: a review, Palaeogeogr. Palaeocl., 281, 269–282, 2009.
Jorgensen, P. M. and Leon-Yanez, S.: Catalogue of the Vascular Plants of Ecuador, Missouri Botanical Garden, Saint Louis, Missouri, USA, 1999.
Jorgensen, P. M. and Ulloa Ulloa, C.: Seed plants of the high Andes of Ecuador. A check list, Dpt. of Systematic Botany, Univ. of Aarhus in coll. with Dpto Ciencias Biologicas, PUCE, Quito, Ecuador, 1994.
Jöris, O. and Weninger, B.: Extension of the ^{14}C calibration curve to ca. 40,000 cal BC by synchronizing Greenland ^{18}O/^{16}O ice core records and North Atlantic foraminifera profiles: A comparison with U/Th coral data, Radiocarbon, 40, 495–504, 1998.
Kuentz, A.: Dynamiques actuelle et holocène de la puna (Andes sèches du Pérou) à partir des observations de terrain, de la cartographie (SIG) et de la palynologie (région du Nevado Coropuna), Université Blaise Pascal, Clermont-Ferrand, 256 pp., 2009.
Kuentz, A., Ledru, M.-P., and Thouret J. C.: Environmental changes in the highland of the Western Andean Cordillera (South Peru) during the Holocene, The Holocene, in press, 2012.
Liu, K.-B., Reese, C. A., and Thompson, L. G.: Ice-core pollen record of climatic changes in the Central Andes during the last 400 yr, Quaternary Res., 64, 272–278, 2005.
Mann, M. E., Zhang, Z., Rutherford, S., Bradley, R. S., Hughes, M. K., Shindell, D. T., Ammann, C., Faluvegi, G., and Ni, F.: Global signatures and dynamical origins of the Little Ice Age and Medieval Climate Anomaly, Science, 326, 1256–1260, 2009.
Marengo, J. A.: Long-term trends and cycles in the hydrometeorology of the Amazon Basin since the late 1920's, Hydrol. Process., 23, 3236–3244, 2009.
Marengo, J. A. and Nobre, C. A.: General characteristics and variability of climate in the Amazon Basin and its links to the global climate system, in: The Biogeochemistry of the Amazon Basin, edited by: Mcclain, M. E., Victoria, R. L., and Richey, J. E., Oxford University Press, Oxford, 2001.
McCormac, G., Hogg, A., Blackwell, P., Buck, C., Higham, T., and Reimer, P.: SHcal04 Southern Hemisphere calibration 0–11.0 cal kyr BP, Radiocarbon, 46, 1087–1092, 2004.

CPD
8, 4295–4332, 2012

Morales, M. S., Christie, D. A., Villalba, R., Argollo, J., Pacajes, J., Silva, J. S., Alvarez, C. A., Llancabure, J. C., and Soliz Gamboa, C. C.: Precipitation changes in the South American Altiplano since 1300 AD reconstructed by tree-rings, Clim. Past, 8, 653–666, doi:10.5194/cp-8-653-2012, 2012.

Moscol Oliveira, M. and Hooghiemstra, H.: Three millennia upper forest line changes in Northern Ecuador: pollen records and altitudinal vegetation distributions, Rev. Palaeobot. Palynol., 163, 113–126, 2010.

Mothes, P. A. and Hall, M. L.: The plinian fallout associated with Quilotoa's 800 yr BP eruption, Ecuadorian Andes, J. Volcanol. Geoth. Res., 176, 56–69, 2008.

Moy, C. M., Seltzer, G. O., Rodbell, D. T., and Anderson, D. M.: Variability of El Niño/Southern Oscillation activity at millennial timescales during the Holocene epoch, Nature, 420, 162–165, 2002.

Neukom, R. and Gergis, J.: Southern Hemisphere high-resolution palaeoclimate records of the last 2000 years, The Holocene, 22, 501–524, 2012.

Ortuño, T.: Relation végétation pollen climat dans les écorégions de Bolivie, Master FENEC, University of Montpellier 2, France, 45 pp., 2008.

Ortuño, T., Ledru, M.-P., Cheddadi, R., Kuentz, A., Favier, C., and Beck, S.: Modern pollen rain, vegetation and climate in Bolivian ecoregions, Rev. Palaeobot. Palynol., 165, 61–74, 2011.

Polissar, P. J., Abbott, M. B., Wolfe, A. P., Bezada, M., Rull, V., and Bradley, R. S.: Solar modulation of Little Ice Age climate in the tropical Andes, P. Natl. Acad. Sci. USA, 103, 8937–8942, 2006.

Reese, C. A. and Liu, K.-B.: A modern pollen rain study from the Central Andes region of South America, J. Biogeogr., 32, 709–718, 2005.

Reuter, J., Stott, L., Khider, D., Sinha, A., Cheng, H., and Edwards, R. L.: A new perspective on the hydroclimate variability in Northern South America during the Little Ice Age, Geophys. Res. Lett., 36, L21706, doi:10.1029/2009GL041051, 2009.

Robin, C., Samaniego, P., Le Pennec, J. L., Fornari, M., Mothes, P., and van der Plicht, J.: New radiometric and petrological constraints on the evolution of the Pichincha volcanic complex (Ecuador), B. Volcanol., 72, 1109–1129, 2010.

Rodbell, D. T., Seltzer, G. O., Anderson, D. M., Abbott, M. B., Enfield, D. B., and Newman, J. H.: An ~15 000-year record of El Niño-driven alluviation in Southwestern Ecuador, Science, 283, 516–520, 1999.

CPD
8, 4295–4332, 2012

Romoleyroux, K.: Extensión y Biodiversidad florística de los Bosques de *Polylepis* en Oyacachi, Noreste del Ecuador Diciembre 2008–Junio 2009, project report, PUCE, Quito, Ecuador, 2009.

Samaniego, P., Robin, C., Chazot, G., Bourdon, E., and Cotten, J.: Evolving metasomatic agent in the Northern Andean subduction zone, deduced from magma composition of the long-lived Pichincha volcanic complex (Ecuador), Contrib. Mineral Petr., 160, 239–260, 2010.

Sachs, J. P., Sachse, D., Smittenberg, R. H., Zhang, Z., Battisti, D. S., and Golubic, S.: Southward movement of the Pacific intertropical convergence zone ad 1400–1850, Nat. Geosci., 2, 519–525, 2009.

Seager, R., Burgman, R., Kushnir, Y., Clement, A. C., Cook, E. R., Naik, N., and Miller, J.: Tropical Pacific forcing of North American medieval megadroughts: testing the concept with an atmopshere model forced by coral-reconstructed SSTs, J. Climate, 21, 6175–6190, 2008.

Stuiver, M. and Reimer, P. J.: Extended ^{14}C data base and revised calib 3.0 ^{14}C age calibration program, Radiocarbon, 35, 215–230, 1993.

Stuiver, M., Reimer, P. J., Bard, E., Beck, J. W., Burr, G. S., Hughen, K. A., Kromer, B., McCormac, F. G., and Van Der Plicht, J.: Intcal 98 radiocarbonage calibration 24 000–0 cal BP, Radiocarbon, 40, 1127–1151, 1998.

Stuiver, M., Reimer, P. J., and Reimer, R.: Calib radiocarbon calibration program rev.6.0.1, available at: http://www.calib.qub.ac.uk/calib, Radiocarbon, 35, 215–230, 2011.

Urrutia, R. and Vuille, M.: Climate change projections for the Tropical Andes using a regional climate model: temperature and precipitation simulations for the end of the 21st century, J. Geophys. Res., 114, D02108, doi:10.1029/2008JD011021, 2009.

Vimeux, F., Ginot, P., Schwikowski, M., Vuille, M., Hoffmann, G., Thompson, L. G., and Schotterer, U.: Climate variability during the last 1000 years inferred from Andean ice cores: a review of methodology and recent results, Palaeogeogr. Palaeocl., 281, 229–241, 2009.

Vuille, M., Bradley, R. S., and Keimig, F.: Climatic variability in the Andes of Ecuador and its relation to tropical Pacific and Atlantic sea surface temperature anomalies, J. Climate, 13, 2520–2535, 2000.

Vuille, M., Burns, S. J., Taylor, B. L., Cruz, F. W., Bird, B. W., Abbott, M. B., Kanner, L. C., Cheng, H., and Novello, V. F.: A review of the South American monsoon history as recorded in stable isotopic proxies over the past two millennia, Clim. Past, 8, 1309–1321, doi:10.5194/cp-8-1309-2012, 2012.

CPD
8, 4295–4332, 2012

Table 1. Chronology of core PA 1-08. Radiocarbon ages were measured on total organic matter. Calibrated ages were calculated from Calib 6.01 (Stuiver et al., 1998; Jöris and Weninger, 1998).

Lab number	Depth in cm	Age ^{14}C yr B.P.	cal yr AD*
SacA 11045	22–24	0	2000
SacA 18852	50–52	175 ± 30	1734–1782 1758
Beta 243042	80–82	270 ± 40	1523–1666 1594
SacA 14722	114–116	530 ± 30	1399–1432 1415
SacA 14723	160–162	1005 ± 30	991–1037 1014
SacA 14724	254–256	1540 ± 35	

* Range at one standard deviation with error multiplier of 1.0; cal = calibrated.

CPD
8, 4295–4332, 2012

Table 2. Chronology of core PA 1-08 from tephra analyses. The calculated age was obtained from the age model based on radiocarbon dating.

Tephra layer	Depth in cm	Name of the volcano	Date of the eruption	Calculated age
M1	110–115	Guagua Pichincha	1660 AD	1660 AD
M2	130–148	Quilotoa	1270–1280 AD	1220 AD
M3	178–181	Guagua Pichincha	800–1000 AD	1035 AD

CPD
8, 4295–4332, 2012

Table 3. Detailed description of the pollen zones defined in Fig. 5.

Pollen zone	Pollen signature
Zone P8 200–180 cm 921–1017 AD 9 samples	AP (13–27 %) with *Polylepis* (3–7 %) Melastomataceae (1–4 %) and low frequencies of *Alnus* (1–2 %) and *Hedyosmum* (1–4 %). A peak in Urticales at 186 cm followed the M3 eruption. Among the herbs, *Ambrosia* (17–8 %), Asteraceae *Senecio* type (4–14 %), Poaceae (10–27 %), *Gentianella* (2–4 %) are dominants. Ferns showed low frequencies in this zone.
Zone P7 180–165 cm 1017–1126 AD 6 samples	The AP decreased by 11–22.5 % mainly due to a decrease in Melastomataceae (0.5–5 %) and low *Alnus* frequencies (1.5–2.5 %) and *Hedyosmum* (0–3 %). *Polylepis* is well represented (3–8.5 %). This zone is characterized by an increase in Poaceae frequencies (21.5–37.5 %) *Ambrosia* (4.5–9.5 %), and *Gentianella* (1–3 %).
Zone P6 165–126 cm 1126–1291 AD 11 samples	Two sub-zones were distinguished: between 165 and 148 cm in depth. This is the period before the eruption of the Quilotoa with high *Alnus* (2–9 %) and *Hedyosmum* (0–7 %) frequencies, *Polylepis* around 5 %. AP was 15–31 %. Among the herbs *Gentianella* 0–3 % and Poaceae 22–53 %; between 132 and 126 cm after the eruption of the Quilotoa, a decrease is observed in *Alnus* and *Hedyosmum* with 0.5 and 1 % respectively and AP was 10–16 %. For the first time since the base of the record, *Polylepis* showed low frequencies, i.e. 0 % at 132 cm and 3 % at 128 cm. *Senecio* type Asteraceae became the dominant taxa (22–33 %) and lower frequencies of Poaceae than before the eruption were observed. An increase of 11 % in *Gunnera* and spores of *Huperzia* (6–16 %) also characterized this zone P6.
Zone P5 126–95 cm 1291–1500 AD 12 samples	There was a general increase in tree frequencies of from 9 to 15 %. However, within this zone, the M1 eruption had consequences for a few taxa such as a sharp increase in *Alnus* frequencies that was observed in the second half of the zone after the M1 eruption. High frequencies of Melastomataceae (4 %) and a decrease at a depth of 110 cm during the M1 eruption were observed. Among the herbs, we noted the absence of *Ambrosia*, an 11–23 % increase in *Senecio* type Asteraceae, *Gentianella* (2–10 %), the Poaceae (20–38 %), the disappearance of *Gunnera*, and increase in *Baccharis* type Asteraceae after the eruption and an increase in *Huperzia* ferns (10–58 %).
Zone P4 95–60 cm 1500–1730 AD 16 samples	There was an 11–24 % increase in tree frequencies, the presence of *Alnus* (1–3.5 %), *Polylepis* were well represented (3–11 %), a decrease in Poaceae, and a progressive increase in Apiaceae (1–14 %) at the end of the zone and presence of *Ambrosia* (0–6 %), a continuous increase *Baccharis* type Asteraceae (10–25 %), the presence of *Gentianella* (1–10 %) and *Huperzia* 15–47 %.
Zone P3 60–28 cm 1725–1960 AD 11 samples	Tree frequencies were higher than in the previous zone with 16 to 37 % mainly *Alnus* and *Hedyosmum* 4–9 % *Polylepis* was well represented 3–6 %. For herbs, an increase in *Ambrosia* (1–12 %), a decrease in Apiaceae (3–19 %), the presence of Ericaceae 1–5 %, low frequencies of *Gentianella* 0–5 % and Poaceae 17–7 %, a sharp increase (20–97 %) in the *Huperzia* fern were observed.
Zones P1–P2 28–0 cm 1960–2008 AD 11 samples	AP 34–46 % with *Alnus* 6–16 %, *Hedyosmum* 4–9 % and *Polylepis* 5–7 %. Among the NAP we observed *Senecio* type Asteraceae (11–18 %), *Ambrosia* (5–14 %), Apiaceae (2–3 %), Ericaceae 2–8 %, *Gentianella* 3 % and *Huperzia* up to 405 %.

CPD
8, 4295–4332, 2012

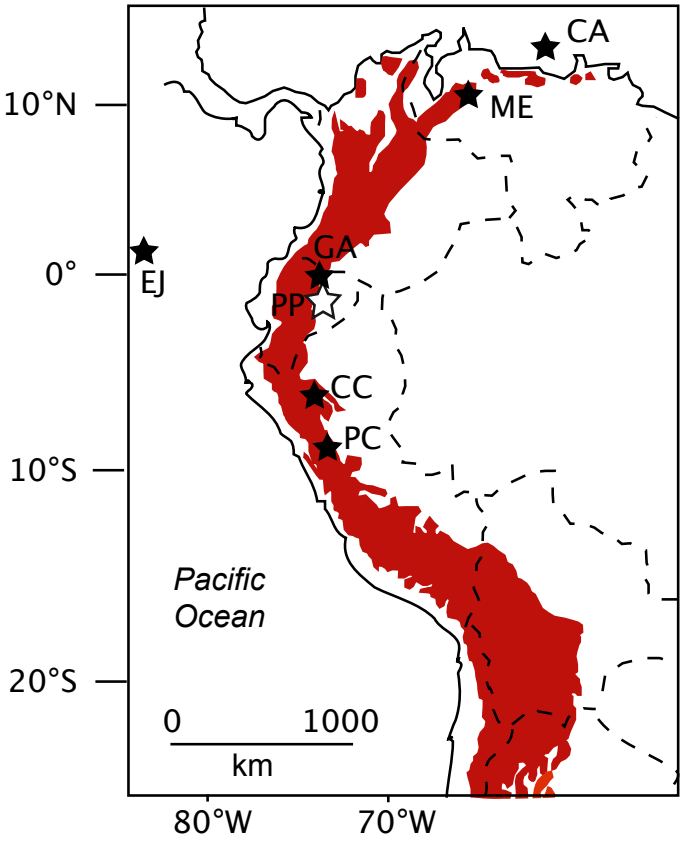

Fig. 1. Map of Western South America showing the tropical Andes (in red) and the locations of records discussed in the text (EJ, lake of El Junco; CA, Cariaco Basin; ME, Andes of Merida; GA, bog of Guandera; PP, bog of Papallacta; CC, Cascayunga Cave, PC, lake of Pumacocha).

CPD
8, 4295–4332, 2012

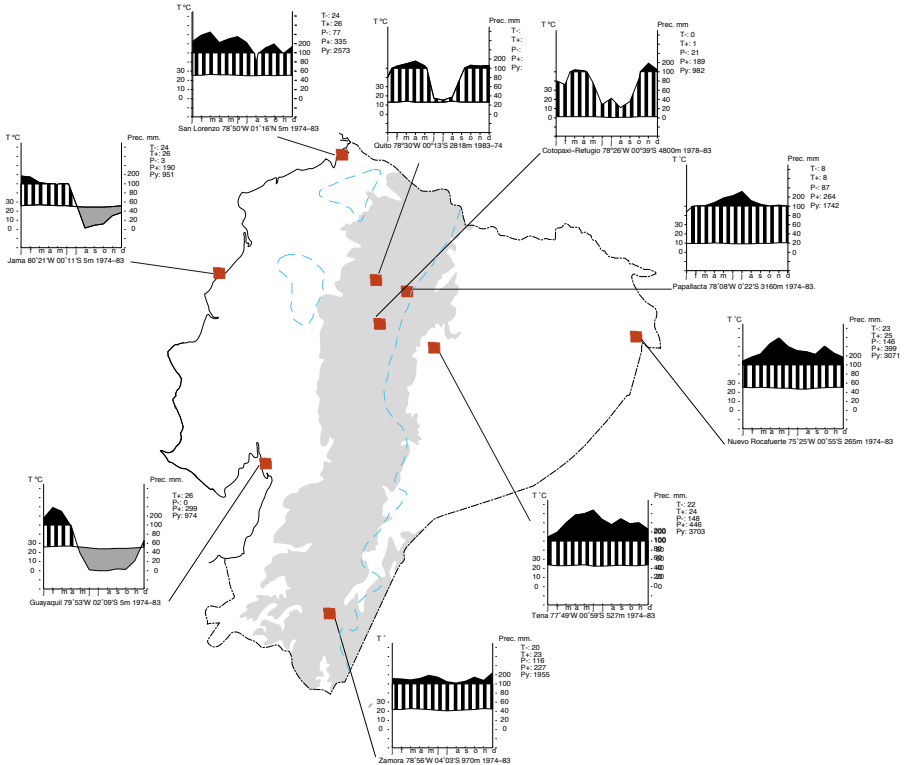

Fig. 2. Map of Ecuador with the 2500 m altitudinal limit (blue line) and climate diagrams drawn for the different regions (from Jorgensem and Ulloa Ulloa, 1994).

CPD
8, 4295–4332, 2012

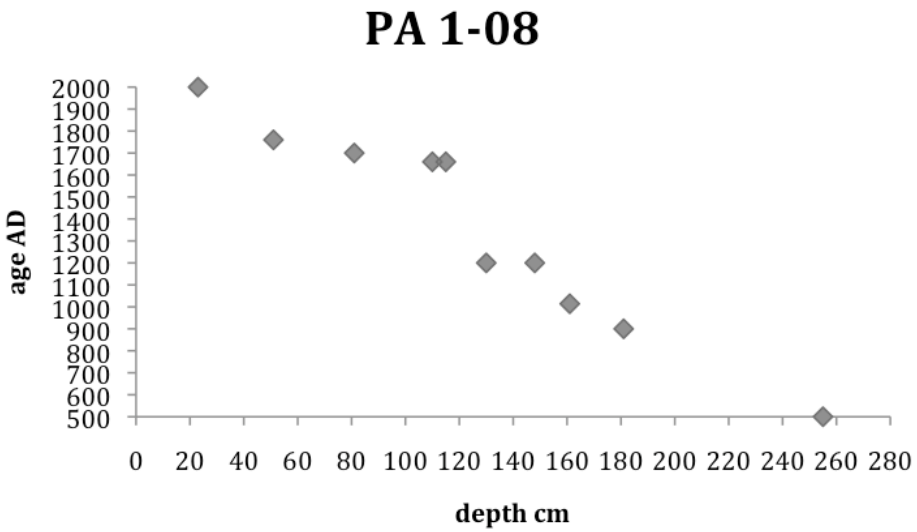

Fig. 3. Age/depth curve for the core PA 1-08 that shows the age model used for the chronology of core PA 1-08 with respectively between 200 and 150 cm, $y = -6.1058x + 2040.7$; between 138 and 115 cm, $y = -30.667x + 5186.7$; between 15 and 0 cm, $y = -3.3116x + 2007.7$.

CPD
8, 4295–4332, 2012

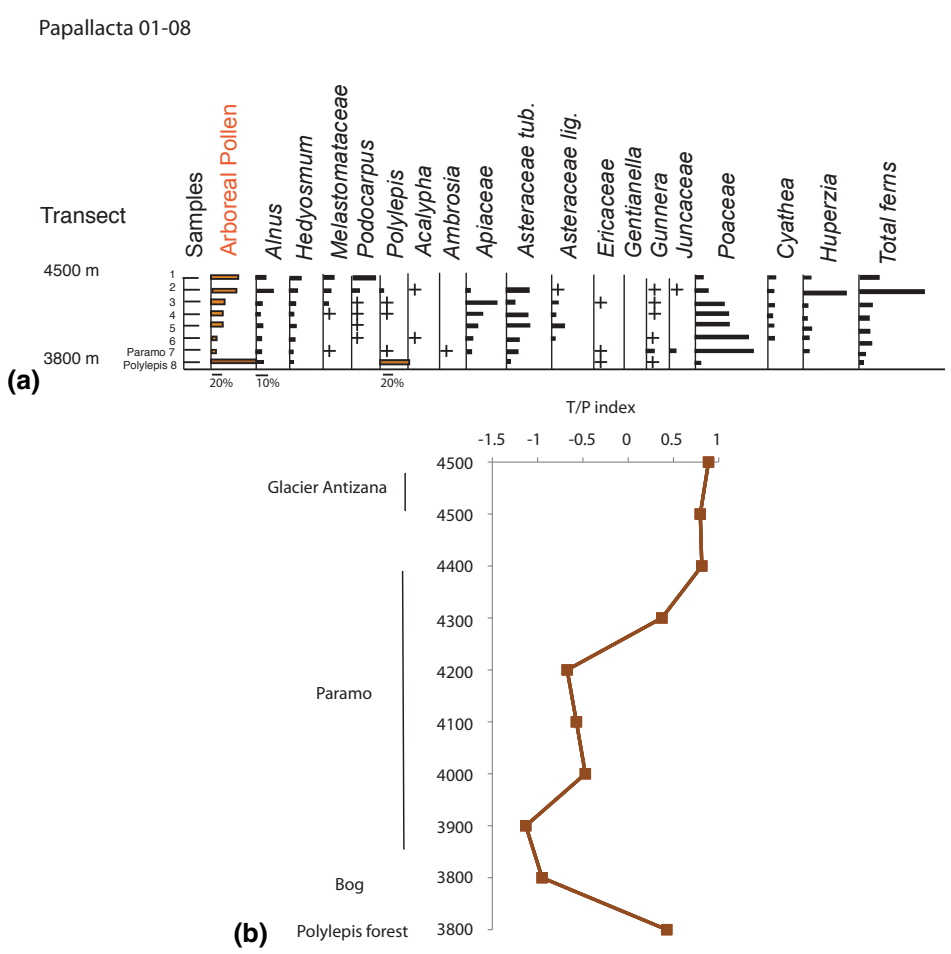

Fig. 4. (a) Pollen diagram showing the modern pollen rain along a transect between Antizana glacier (4500 m) and Papallacta bog (3800 m) for the main taxa. **(b)** T/P index of convectivity for surface samples along the altitudinal transect.

CPD
8, 4295–4332, 2012

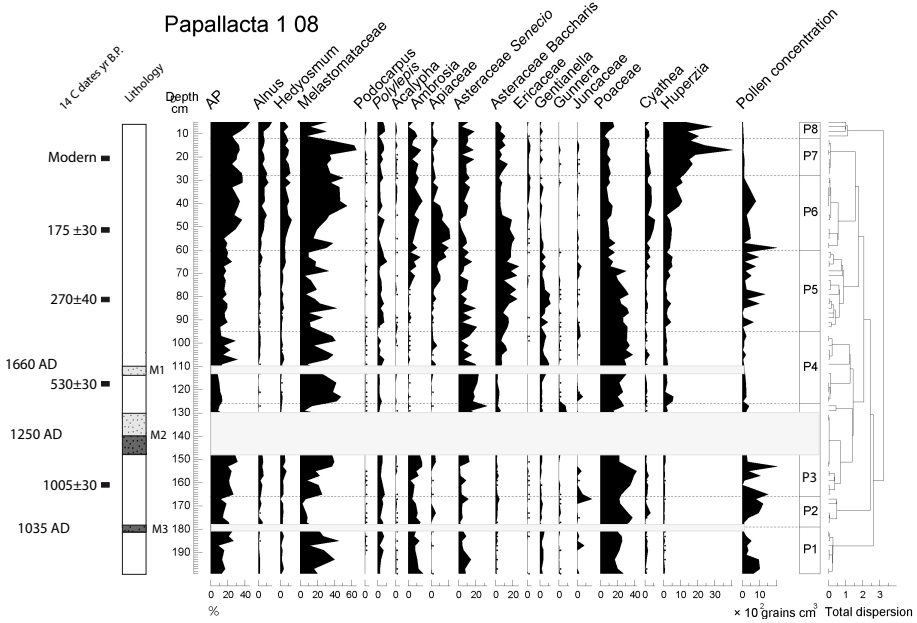

Fig. 5. Synthetic pollen diagram of core PA 1-08. Changes in arboreal pollen and 17 key taxa are presented along a depth scale. See detailed lithological description in the text.

CPD
8, 4295–4332, 2012

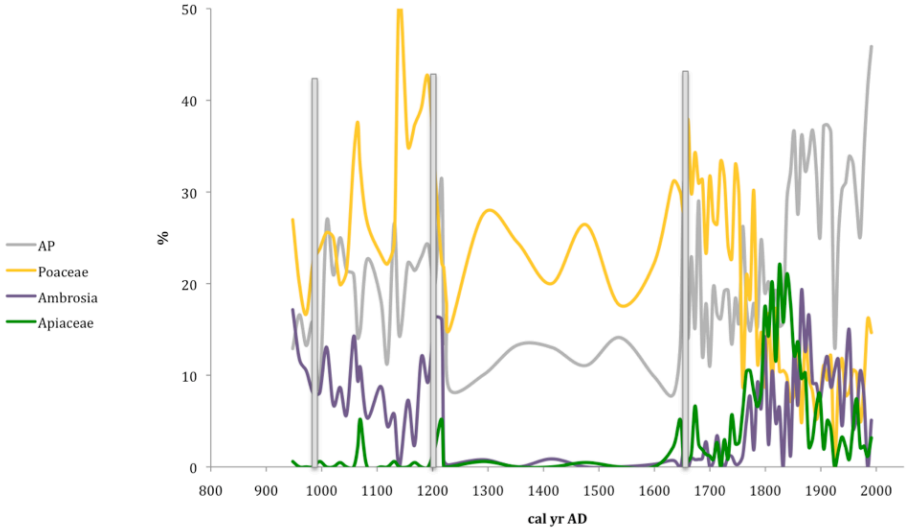

Fig. 6. Synthetic pollen diagram of core PA 1-08 showing changes in frequencies of arboreal pollen taxa, Poaceae, *Ambrosia* and Apiaceae presented along a time scale. Gray bars indicate volcanic eruptions.

CPD
8, 4295–4332, 2012

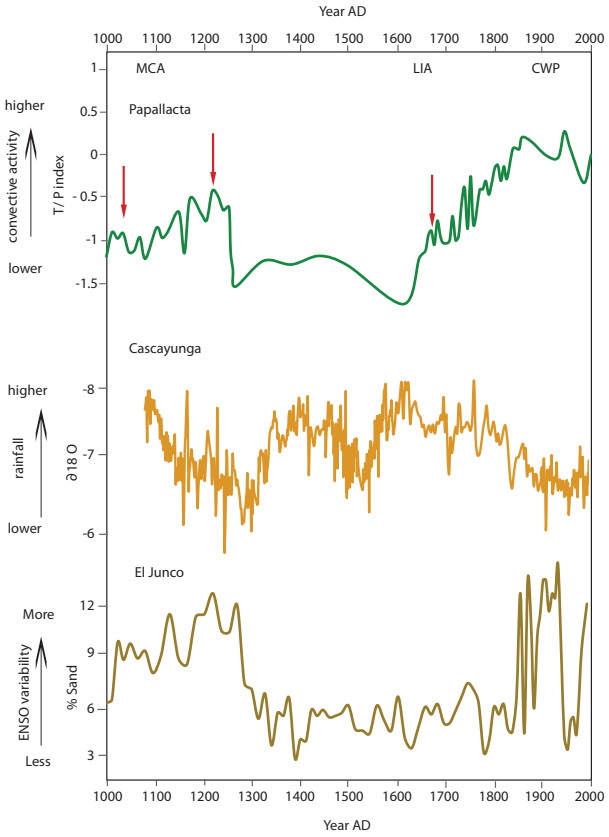

Fig. 7. The past 1000 yr in western South America with **(A)** the Papallacta T/P index of upslope convectivity calculated from the PA 1-08 pollen record; **(B)** ∂18O cal from Cascayunga, Peru, a record of SASM intensity (Reuter et al., 2009) and **(C)** % sand from El Junco, Galapagos, a record of El Niño frequencies (from Conroy et al., 2009). Red arrows show volcanic eruptions at Papallacta.

CPD
8, 4295–4332, 2012